Chapter 9

Ultra-Low-Noise Seismic Accelerometers for Earthquake Prediction and Monitoring

Felix A. Levinzon

Additional information is available at the end of the chapter

http://dx.doi.org/10.5772/65925

Abstract

The design of ultra-low-noise seismic piezoelectric accelerometers (PEs) with integral electronics (IEPE) is presented. They feature probably the lowest noise floor (for their size and weight) and the lowest operating frequencies (near-dc) ever reported to date among these types of vibration sensors. These highly sensitive sensors can be used for earthquake monitoring and in the earthquake prediction system by detecting and monitoring microseismic fluctuations. The warning system using these sensors would be fundamentally different from current warning systems using the network of hundreds of seismometers across seismically active regions and recording only seismic events. Two Meggitt (OC) IEPE seismic accelerometers, models 86 and 87-10 having sensitivity of 10 V/G, are described. The model 86 has a weight of about 770 g and a frequency range from 0.003 to 200 Hz at the ±3 dB level. Its noise floor in terms of the equivalent input noise acceleration spectral density is about 37, 7, and 3 nG/$\sqrt{\text{Hz}}$ at at frequencies 1, 10, and 100 Hz, respectively. The model 87-10 is a compact sensor with a weight of about 170 g and a frequency range from 0.02 to 500 Hz at the ±3 dB level. It has noise of about 90, 25, and 10 nG/$\sqrt{\text{Hz}}$ at at frequencies 1, 10, and 100 Hz, respectively.

Keywords: seismic, microseismic, earthquake prediction, earthquake monitoring, accelerometer, low-noise accelerometer, amplifier, low-noise amplifier, piezoelectric

1. Introduction

During an earthquake, the forces and the motion of a point on the ground vary a lot and keep changing. Earthquakes can be so small or distant (for example, in the ocean), that only low-noise or ultra-low-noise sensors are capable of measuring and monitoring small acceleration signals generated by such earthquakes [1–5]. In addition, such sensors can be used for the warning prediction system by detecting and monitoring of "preseismic" small changes on the ground that indicate that a significant quake is imminent [1, 5–9]. Ultra-low-noise seismic

piezoelectric accelerometers with integral electronic (IEPE), also called integral electronic piezoelectric accelerometers or integrated circuit piezoelectric (ICP) accelerometers, are the best candidates for such purposes [10–17]. The advantages of the IEPE accelerometers include high sensitivity, wide dynamic, frequency, and temperature ranges, low output impedance, low noise, and availability of miniature designs. In addition to seismology and earthquake-related measurements, they are used in many applications such as aircraft and automobiles, structure monitoring, seismic isolation and stabilization platforms, homeland security, and oil and mineral exploration.

The earthquake prediction experiments led by the Rice University (Houston, Texas, USA) team and conducted along the San Andreas Fault in Southern California is an example of the use of the ultra-low-noise seismic IEPE accelerometers [1]. Specifically, in one of these experiments, they placed a device that produced seismic waves in rocks located near accelerometers. The waves caused small changes in the rocks that were detected by accelerometers. Those changes were followed by small earthquakes on two occasions. One of these earthquakes occurred about 10 h later. These experiments suggest that low-noise accelerometers located in the right place can pick up potentially worrisome movements in a fault. The study indicated that the stresses measured by such sensors preceded the temblor itself. As a result, a warning system using these sensors can be more effective, in comparison to the warning system with network of hundreds of seismometers across active seismic region such as Southern California. These networks record only seismic events; they cannot identify "preseismic" changes on the ground signaling that a significant quake is imminent. IEPE seismic accelerometers can be used in the seismic network similar to high-resolution seismic network (HRSN) capable of detecting microseismic fluctuations [3, 5–9].

An accelerometer is a vibration sensor that measures acceleration directly proportional to the force applied to an object that causes it to change its position or speed. In seismology, the most common sensor is the seismometer, which measures the velocity of a point on the ground during earthquake. Accelerometers, in contrast to the seismometers, give information about forces that a subject experiences during a seismic activity. Also, they are handy sensors having small size, usually <100 mm on a side, so they can be easily placed at key locations in a structure. Acceleration signals can be integrated by an integrator or by a computer to obtain the velocity and displacement signals. Low-noise accelerometers can be used both for the measurement of small acceleration signals directly and, as the first, low-noise stage of the instruments measuring low-noise velocity signals.

IEPE accelerometers represent the class of dynamic vibration sensors incorporating a piezoelectric (PE) transducer, as a mechanical part, and integral electronics (typically, voltage or charge amplifier), as an electrical part, into one shielded package. **Figure 1** shows the block diagram of the typical IEPE accelerometer and signal conditioning circuit (SCC) connected to the accelerometer with a coaxial cable and typically located outside of the accelerometer [16].

The PE transducer is comprised of a mass m and piezoelectric element often called a crystal. When the input acceleration signal a is applied to the sensor, the mass m imposes a force F on the crystal element, which transforms the input acceleration signal into a charge electrical signal at the output of the PE transducer. The charge signal is amplified by the IEPE sensor

http://dx.doi.org/10.5772/65925

electrical circuit and is converted to a voltage electrical signal at the sensor's output. The sensor measures acceleration signal in accordance with the Newton's second law of motion: $F = ma$.

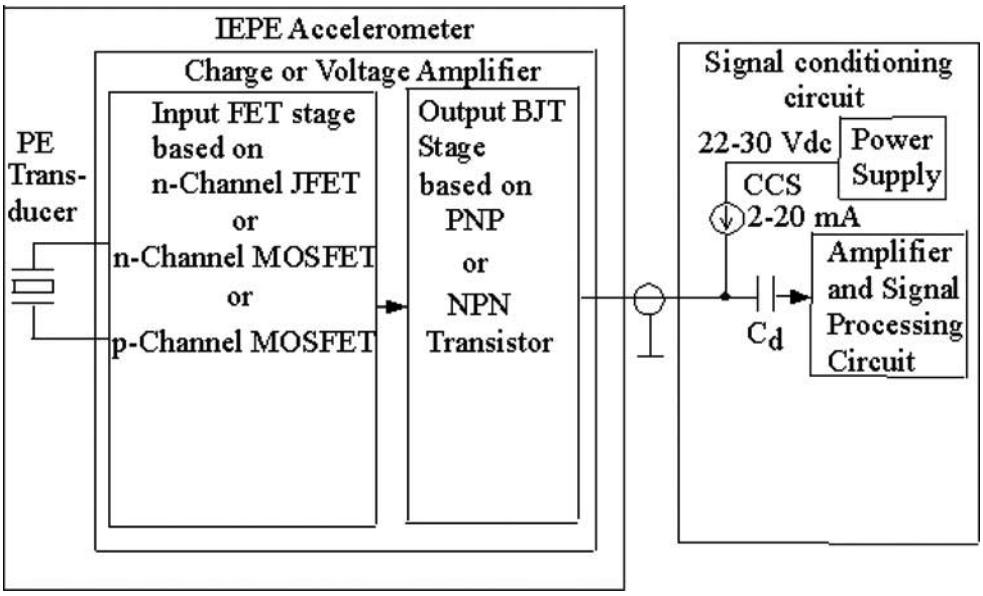

Figure 1. The block diagram of the typical IEPE accelerometer and signal conditioning circuit [16].

The integral electronics of the IEPE accelerometer is comprised of a built-in charge or voltage amplifier which transfers the PE transducer's high impedance into the amplifier's low output impedance allowing transmission of the signal over long cable lengths. The amplifier input stage is based on a field effect transistor (FET) having high input impedance matching the PE transducer's high output impedance. FET type can be typically of n-channel JFET, n-channel MOSFET, or p-channel MOSFET. The output stage is built based on a bipolar junction transistor (BJT) providing low output impedance. BJT can be of PNP or NPN type. Some IEPE sensors have amplifiers containing additional stages between input and output stages.

The signal condoning circuit (SCC) provides power for the accelerometer, additional amplification of the signal coming from accelerometer, and its processing dictated by the sensor applications. Specifically, it can contain an integrator which transforms an acceleration signal into a velocity signal. The integrator can also be placed inside the IEPE sensor if its dimensions allow. Typical voltage supply is from +22 to +30 V_{dc} and current supply is from 2 to 20 mA. The current supply is provided by a constant current source (CCS), which, for example, can be created by a current-regulating diode. A decoupling capacitor C_d eliminates any influence of the IEPE sensor's output dc bias voltage on the SCC input amplifier's stage. This construction allows to have only two wires (signal output and signal ground) for connection of the IEPE accelerometer with the SCC. These wires carry both the accelerometer output signal and voltage supply at the same time.

The sensor operation frequencies, typically from 1 Hz to 10 kHz, are located below the PE transducer's resonant frequency. At these frequencies, the PE transducer-simplified equivalent schematic can be represented as a capacitive signal source having high impedance. **Figure 2** shows the PE transducer-simplified equivalent electrical schematic comprising the signal source electromotive force (EMF), e_{PE} connected in series with capacitor C_{PE} [16]. C_{PE} is the PE transducer's electrical capacitance. e_{PE} represents the output voltage of the open-circuit PE transducer:

$$e_{PE} = a_s \cdot V_{PE}, V_{PE} = \frac{Q_{PE}}{C_{PE}}, q_{PE} = e_{PE} \cdot C_{PE}. \quad (1)$$

In Eq. (1), V_{PE} and Q_{PE} are the PE transducer's voltage sensitivity and charge sensitivity, respectively. q_{PE} is the charge at the output of the PE transducer and a_s is the inputacceleration.

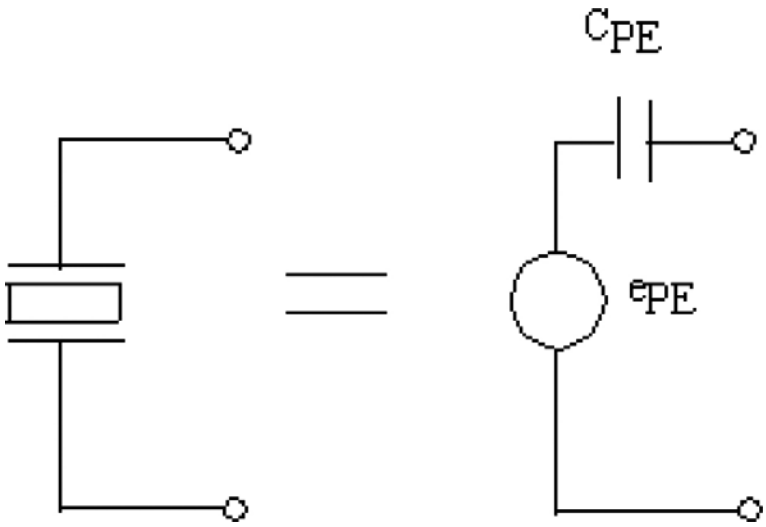

Figure 2. Simplified equivalent schematic of the PE transducer [16].

The IEPE seismic accelerometers are specially designed to measure ultra-low level vibrations at low frequencies (often including frequencies below 1 Hz). These frequencies are associated with earth tremors, large structures, and foundation [10–16]. Some of these accelerometers have frequency response from very low frequency $f \leq 0.01$ Hz. They feature very low noise floor (i.e., estimated at a few dozen $nG/\sqrt{\text{Hz}}$ at frequency 1 Hz and a few $nG/\sqrt{\text{Hz}}$ at frequencies $f \geq 100\text{Hz}$), and high sensitivity (often 1 and 10 V/G), in comparison to other IEPE sensors [15–17]. There are several types of seismic accelerometers that vary in the construction and operating principle. In addition to the IEPE type mentioned above, they can be designed as variable capacitance MEMS [18, 19], and folded pendulum accelerometers [20, 21]. The IEPE and MEMS seismic accelerometers are the types that are most widely used in the industry. Besides seismology and earthquake-related measurements, the applications where they are

http://dx.doi.org/10.5772/65925

used, include isolation and stabilization platforms [15, 16, 20], large structure monitoring [20], spacecraft environmental noise measurement [22], and large antenna dynamic measurement [23]. Specifically, the Meggitt (OC) model 86 described below is used in the National Institute of Standards and Technology (NIST) for the stabilization platform carrying the world's most frequency stable laser system used for the atomic clock research conducted by NIST [17].

2. Block diagram, schematic, and construction of the designed IEPE seismic accelerometers

2.1. Block diagram and schematic of the designed accelerometers

Figure 3 shows photographs of the designed accelerometers, models 86 and 87 [10, 13]. They have cylindrical shape and two-pin connectors. The larger sensor model 86 has a weight of about 770 g, a diameter of about 65 mm, and a height of about 56 mm [10]. The model 87 is compact in weight and dimensions. It has a weight of about 170 g, diameter of about 30 mm, and height of about 37 mm [13].

Figure 3. Photographs of the designed accelerometers [10, 13].

Schematic solution of the designed accelerometers was made from a standpoint of providing ultra-low noise, operating frequency range including very low frequencies f<<1 Hz, temperature range from –20 to +100°C, low output impedance $R_{out} \leq 10\,\Omega$, and protection of the circuit against input transients and shocks.

Figure 4 shows the block diagram and schematic of each of the designed accelerometers and signal conditioning circuit (SCC) connected to them with a coaxial cable [15, 16]. The sensors incorporate the high-sensitivity PE transducer and ultra-low-noise charge amplifier.

The charge amplifier amplifies a charge signal coming from the PE transducer and converts it into a voltage output signal. The input stage has high input impedance and the output stage has low output impedance which allows transmission of the voltage signal over long coaxial cable lengths.

In **Figure 4**, the signal source e_{PE} represents the output voltage of the open-circuit PE transducer. C_{PE} is the PE transducer electrical capacitance. The resistive divider $R1/R2$ and the biasing resistor R_b form the negative dc feedback circuit providing the circuit stable operation and the dc bias voltage for the JFET. C_f is the charge amplifier's feedback capacitance. The value of C_f is selected to provide the necessary charge gain of the amplifier and corresponding sensitivity of the whole sensor.

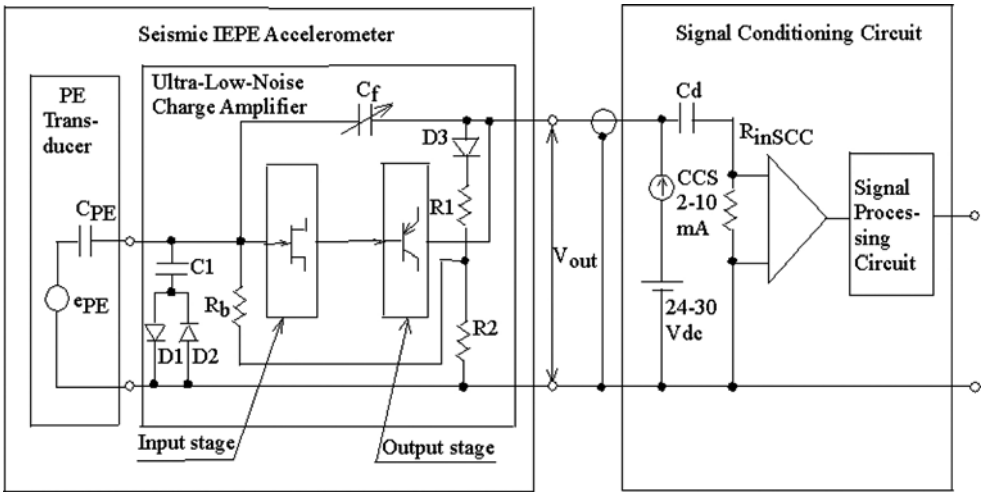

Figure 4. Block diagram and schematic of the designed IEPE seismic accelerometers and signal conditioning circuit [15, 16].

The charge amplifier is comprised of two direct-coupling stages: the input stage based on low-noise JFET and the output stage based on the bipolar transistor BJT. The latter is arranged in the Darlington configuration that makes it possible to provide the sensor's output impedance $R_{out} \leq 10\Omega$. This value is approximately one order of magnitude less, in comparison to the best existing IEPE seismic accelerometers [11, 12]. We can see that the charge amplifier is based on the two discrete transistors, FET and BJT, in comparison to the typical charge amplifier based

http://dx.doi.org/10.5772/65925

on op-amp with a feedback capacitor. Contrary to an op-amp charge amplifier, a FET-BJT charge amplifier can provide lower noise, higher temperature range, smaller size, and two wires output configuration.

The resistors *R*1 and *R*2 and diode *D*3 having negative temperature coefficient form negative feedback circuit for the JFET stage that provides temperature compensation for the JFET temperature drift [15]. It is known that JFET gate current leakage I_{GSS} flowing through the biasing resistor R_b of high value grows exponentially with temperature. As a result, the JFET gate-source voltage V_{GS} increases with temperature as well. This may cause unstable operation of the amplifier. When the temperature changes, the circuit mentioned above changes V_{GS} in the direction opposite to that caused by the JFET leakage current. This schematic solution made possible extending the temperature range of the sensors up to 100°C. In comparison, the current state-of-the-art IEPE seismic accelerometers have operating temperature of ≤65°C [11, 12].

The frequency response lower corner f_L for the charge amplifier and the whole accelerometer at the level of –3 dB is determined by the high-pass one-pole filter formed by the feedback capacitor *Cf* and the input resistance of the charge amplifier R_{in} [15, 16]:

$$f_L = \frac{1}{2\pi R_{in} C_f}. \tag{2}$$

From the schematic shown in **Figure 4**,

$$R_{in} = R_b \cdot \frac{R1 + R2}{R2}. \tag{3}$$

Using Eq. (3), the Eq. (2) can be rewritten as

$$f_L = \frac{1}{2\pi\left(R_b \cdot \frac{R1+R2}{R2}\right) C_f}. \tag{4}$$

To provide $f_L \ll 1\text{Hz}$, resistor R_b needs to be a high value. But, on the other hand, the value of R_b is restricted by the leakage current I_{GSS} of JFET. Thus, it is necessary to choose the optimum value of R_b. The sensor's frequency response in the upper corner is determined by the PE transducer's resonant frequency.

Diodes *D1*, *D*2, and capacitor *C*1 at the input of the JFET stage create the circuit, which provides protection of JFET against shocks and transients coming from the vibration input [15]. Why is it needed to have such protection, even though, typically, JFETs can withstand transient signal of high level? In the IEPE seismic accelerometers, a PE transducer features very high sensitivity. As a result, input vibration transient signals can cause the high magnitude of the voltage transient signals coming to the charge amplifier's input. Such signals may damage JFET. With the purpose to prevent this, the JFET protection circuit mentioned above is included in the amplifier design. One of the diodes *D*1 and *D*2 becomes open, when a transient signal of any polarity is applied to the circuit's input. Then the capacitors *C*1 and C_{PE} create a capacitive divider $C1/C_{PE}$ at the input of the amplifier:

$$G_1 = \frac{1}{1 + \frac{C1}{C_{PE}}}, \qquad G_1 < 1. \tag{5}$$

In Eq. (5), G_1 is the protection circuit's gain (or rather coefficient of transmission, since $G_1 < 1 < 1$). Capacitor $C1$ value is selected so that $C1 = nC_{PE}$. For example, if $n = 9$, $G_1 = 0.1 = 0.1$, and the input transient or shock signal will be reduced by a factor 10. In the designed sensors, the protection circuit allowed providing the shock limit of 250 G pk for the accelerometer model 86 and 400 G pk for the accelerometer model 87. These shock limit values exceed the similar parameter of the existing state-of-the-art IEPE seismic sensors [11, 12].

The SCC is connected with the sensor using a coaxial cable and may be located far from the sensor. The SCC is comprised of an additional amplifier, possibly integrated to convert acceleration signal into velocity, and other stages used for the signal processing. Also, SCC provides the power supply for the charge amplifier. The voltage supply VS can be of any value from 24 to 30 V_{dc}. The current supply is formed by the constant current source CCS and can be from 2 to 10 mA. With the purpose to decrease noise contribution from the power supply, the rechargeable nickel-cadmium (NiCd) battery is used as VS and a current-regulating diode (such as the 1N5312 with the nominal value of 3.9 mA) is used as CCS. The low-noise op-amp (e.g., the OPA27A) is recommended for the SCC amplifier. The time constant τ of the circuit C_d - R_{inSCC} formed by the decoupling capacitor C_d and the input resistor R_{inSCC} of the SCC amplifier should be chosen high enough to provide a flat frequency response and negligible contribution of the thermal noise caused by R_{inSCC}:

$$\tau = C_d \cdot R_{inSCC} \gg \frac{1}{2\pi f_L}. \tag{6}$$

2.2. Construction of the designed accelerometers

Figure 5 shows the construction of the designed accelerometers [15, 16]**.**

The PE transducer is comprised of a crystal support, mass, case, and PE elements (crystals) made of lead zirconate titanate (PZT) piezoceramic material. The mass is built as one piece and consists of two sections: crossbeam section and cylindrical section. The crossbeam section is bonded to the crystals in its center. The sensor's vibration axis coincides with the cylinder axis.

The PE **t**ransducer operates in circular bender, flexural mode typical for the IEPE seismic accelerometers featuring high sensitivity, low resonant frequency, and low pyroelectric effect [24]. When a vibration signal is applied to the sensor's case, the mass and crystals are bending that causes the latters to generate electrical signals. The bender mode construction leads to the motion mechanical amplification resulting in the PE transducer's high values of charge sensitivity Q_{PE} and voltage sensitivity V_{PE}. High values of Q_{PE} and V_{PE} are the key factors in providing the sensors' ultra-low-noise floor [15, 16].

The charge amplifier is built on a ceramic hybrid substrate with gold metallization on the conductors. **Figure 6** shows a photograph of the charge amplifier hybrid substrate [15, 16]. The substrate has the shape of a disk and is placed into the inner shielded case. The inner case is isolated from the sensor's outer case to prevent ground loops that can occur when the sensor

http://dx.doi.org/10.5772/65925

is connected to the remotely distant SCC. The components have either surface mount technology (SMT) package or die (chip) form used for the wirebond connection. All components are attached to the substrate using conductive and insulative epoxies.

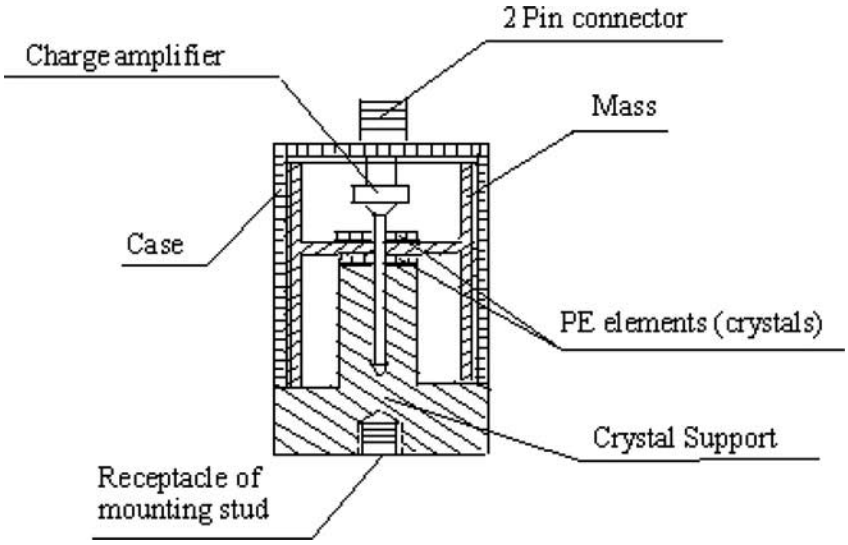

Figure 5. Construction of the designed accelerometers [15, 16].

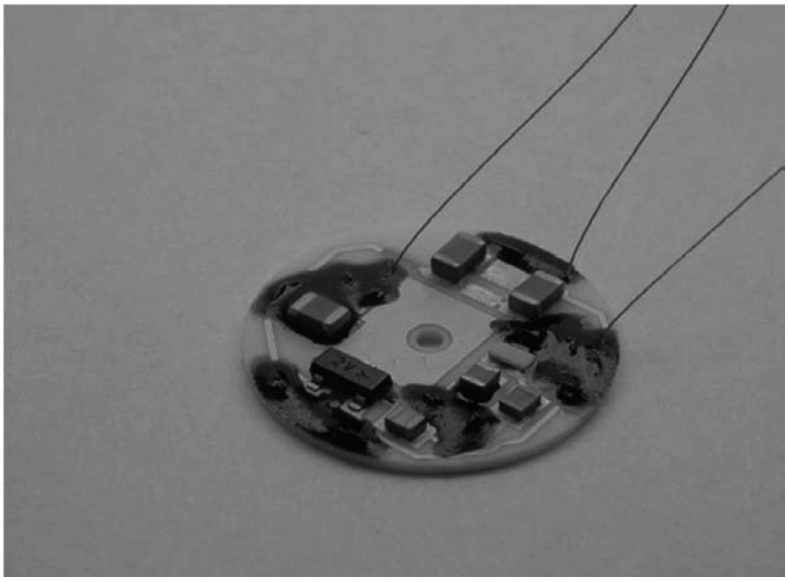

Figure 6. Photograph of the charge amplifier hybrid substrate [15, 16].

The gold wirebonds are used for connecting the die components with the substrate gold conductors. Both wirebonds and die components are coated by an isolative coating epoxy to protect them against possible damage during sensor assembly. Connections between the hybrid substrate, the output two-pin connector, and the PE transducer are made with the help of three gold wires attached to the substrate and covered with an isolation material.

3. Performance characteristics of the designed accelerometers

Table 1 shows the typical performance characteristics of the designed accelerometers, models 86 and 87 [10, 13].

Performance characteristics	**Units**	**Model 86**	**Model 87**	
			87-1	**87-10**
Voltage sensitivity	V/G	10	1	10
Range (max level measured)	G	±0.5	±5	±0.5
Frequency response at level of the ±1 dB	Hz	0.005– 100	0.02–380	0.05–380
Frequency response at level of the ±3 dB	Hz	0.003–200	0.01–500	0.02–500
Resonant frequency	Hz	370	1220	1220
Output bias voltage	V_{dc}	+8–+13	+8–+13	+8–+13
Temperature range	°C	–20–+100	–20–+100	–20–+100
Full scale output voltage	V	±5	±5	±5
Output impedance, R_{out}	Ω	≤10	≤10	≤10
Noise (equivalent input noise acceleration):				
Broadband (1 Hz–1 kHz) noise	nGrms	100	1500	300
Spectral noise:	$nG/\sqrt{Hz}$			
0.1 Hz		600	1000	800
1 Hz		37	170	90
10 Hz		7	36	25
100 Hz		3	20	10
Voltage supply	V_{dc}	+24–+30	+24–+30	+24–+30
Current supply	mA	2–10	2–10	2–10
Shock limit	G pk	250	400	400
Dimensions: diameter	mm (in)	64.8 (2.55)	28.6 (1.125)	28.6 (1.125)
Height	mm (in)	55.5 (2.18)	37.3 (1.47)	37.3 (1.47)
Weight	g (lb)	771 (1.7)	170 (6.0)	170 (6.0)

Table 1. Typical performance characteristics of the designed accelerometers [10, 13].

http://dx.doi.org/10.5772/65925

Model 86 has sensitivity 10 V/G and range (max g-level measured) 0.5 G pk. Model 87 has two modifications: 87-1 and 87-10 having sensitivities of 1 and 10 V/G and ranges between 5 and 0.5 G pk, respectively. **Figures 7** and **8** show frequency response curves of the models 86 and 87-10, respectively [16].

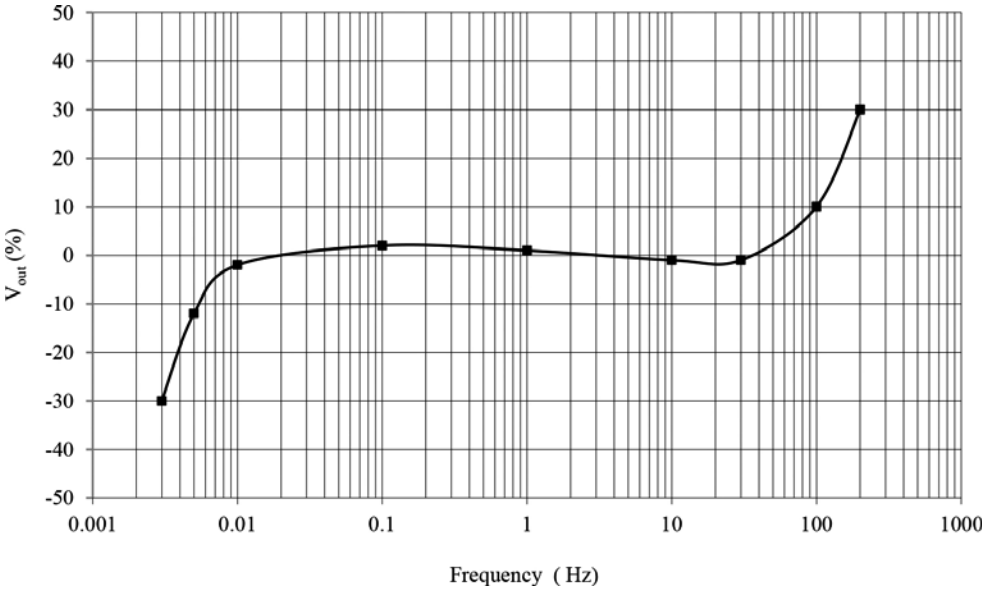

Figure 7. Frequency response of the accelerometer 86 [16].

For the accelerometer model 86, the lower and upper corners of frequency response at the level of ±3 dB are 0.003 and 200 Hz, respectively. For the accelerometers 87-10 and 87-1, those corners are 0.02 and 500 Hz and 0.01 and 500 Hz, respectively. The –3 dB frequency response lower corners are determined by the expression (2). At high frequencies, the sensor's resonance is the main factor for the frequency response rise.

The accelerometers operate over a temperature range from –20°C to +100°C. **Figure 9** shows the typical temperature response which shows the deviation of an accelerometers' sensitivity over operating temperature range [15]. We can see that the temperature response is from –15% at −20°C to +10% at +100°C relatively to 25°C.

In **Table 1**, the spectral noise a_n is shown in terms of equivalent input noise acceleration spectral density (in $nG/\sqrt{\text{Hz}}$). For the model 86, having the lowest noise, a_n was estimated (theoretical noise) as a result of the noise analysis made in [15] and briefly presented below. Theoretical values of a_n for the model 86 were verified by the direct measurement of its noise in NIST (experimental noise) [15, 16].

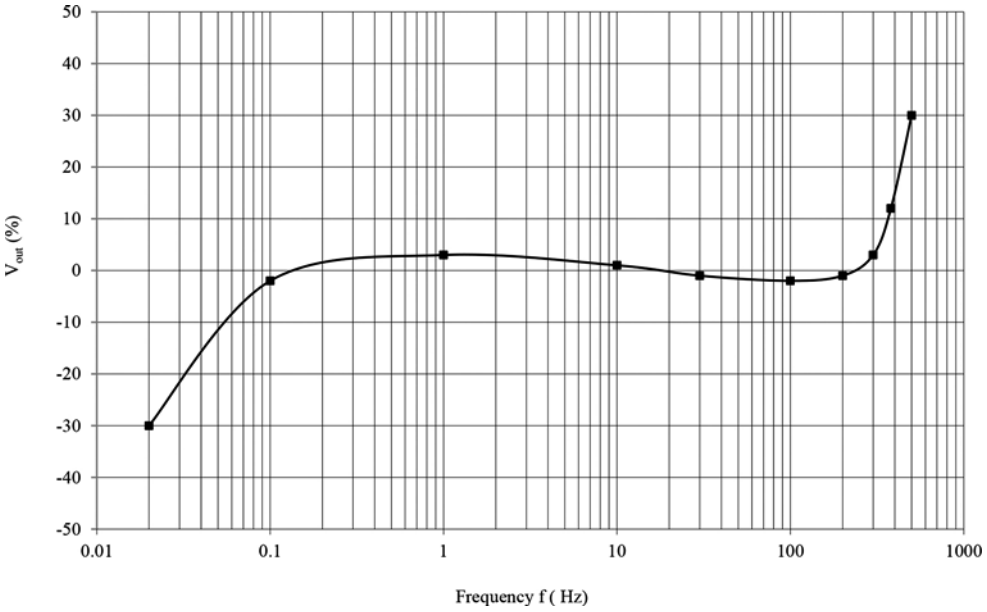

Figure 8. Frequency response of the accelerometer 87-10 [16].

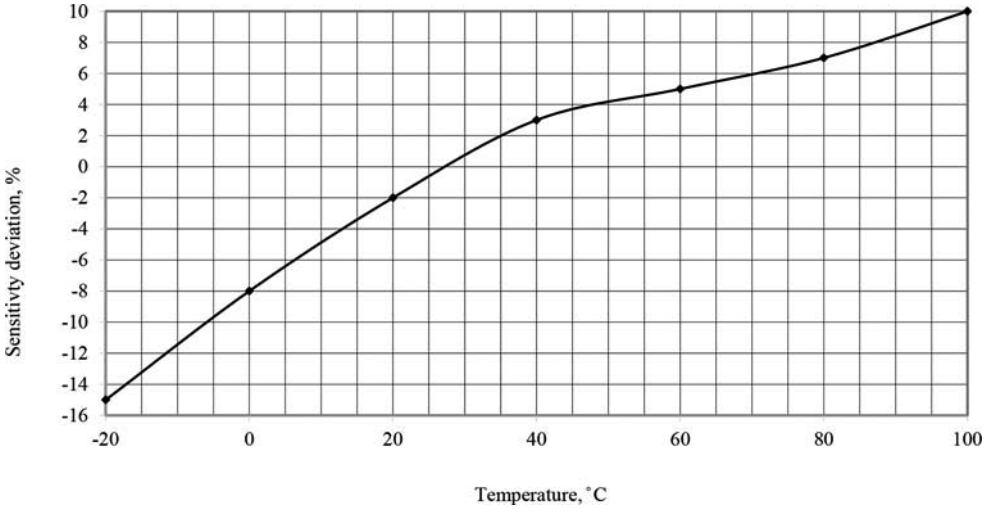

Figure 9. Typical temperature response of the designed accelerometers [15].

http://dx.doi.org/10.5772/65925

4. Noise analysis of the designed accelerometers and the noise measurement results

Spectral noise a_n is a critical parameter of any seismic sensor, because it defines the lowest level of acceleration signal that can be measured at different frequencies of the accelerometer frequency range. Noise analysis of the designed accelerometers was made in [15] based on the equivalent noise circuit of the IEPE accelerometer [16, 25]. For the reader's convenience, we have presented here the basic considerations and the final expression for a_n.

a_n is determined as a sum of the noise contributions of the PE transducer a_{nPE} and the charge amplifier a_{namp} which are not correlated to each other by definition [15, 16]:

$$\overline{a_n{}^2} = \overline{a_{nPE}{}^2} + \overline{a_{namp}{}^2}. \tag{7}$$

Noise of the PE transducer a_{nPE} is supposed as a combination of its electrical-thermal noise a_{ne} and mechanical-thermal noise a_{nm}, which are not correlated to each other by definition [25, 26]:

$$\overline{a_{nPE}{}^2} = \overline{a_{ne}{}^2} + \overline{a_{nm}{}^2} = 4kT\left(\frac{\eta C_{PE}}{\omega Q_{PE}{}^2} + \frac{0.01\omega_0}{mQ}\right). \tag{8}$$

In Eq. (8), k is the Boltzmann's constant (1.38×10^{-23} J/K), T is the absolute temperature in K, $\omega = 2\pi f$, $\omega_0 = 2\pi f_0$, f is a frequency, f_0 is the PE transducer's resonant frequency: η, Q, and m are the PE transducer's loss factor, quality factor, and mass, respectively. In Eq. (8), $\overline{a_{nPE}{}^2}$ is presented in terms of G^2/Hz.

The main noise sources of the FET-input charge amplifier a_{namp} include the noise a_{nFET} generated by FET and the thermal noise a_{nR_b} caused by the biasing resistor R_b [16, 25]

$$\overline{a_{namp}{}^2} = \overline{a_{nFET}{}^2} + \overline{a_{nR_b}{}^2}. \tag{9}$$

a_{nFET} is comprised of the FET noise sources: the channel thermal a_{nt}, $1/f$ noise $a_{n1/f}$, and the shot noise a_{ns} in the gate circuit caused by the gate leakage current I_{GSS}:

$$\overline{a_{nFET}{}^2} = \overline{a_{nt}{}^2} + \overline{a_{n1/f}{}^2} + \overline{a_{ns}{}^2}. \tag{10}$$

The expression for the total equivalent input noise acceleration spectral density a_{namp} contributed by amplifier is [16]

$$\overline{a_{namp}{}^2} = \frac{1}{V_{PE}{}^2}\left\{4kT\frac{\Gamma}{g_{fs}} + \frac{\alpha q V_G{}^*}{2C_{in}f} + \frac{2qI_{GSS}}{(\omega C_{PE})^2} + \frac{4kTR_b}{[1+(\omega R_b C_f)^2]}\left(\frac{C_f}{C_{PE}}\right)^2\right\}. \tag{11}$$

In Eq. (11), Γ is a constant, for most FETs, Γ ≈ 2/3 [27]. g_{fs} is the FET forward transconductance and α is 1/*f* parameter used as a figure of merit for the FET 1/*f* noise. q is the electron charge of 1.6×10^{-19} coulomb, $V_G{}^*$ is the effective gate voltage, and C_{in} is the FET input capacitance.

In Eq. (11), the first term represents the FET channel thermal noise a_{nt}, the second term corresponds to the FET 1/*f* noise $a_{n1/f}$, the third and fourth terms define the FET shot noise a_{ns} in the gate circuit and the thermal noise generated by the biasing resistor R_b, respectively.

By substituting noise items in Eq. (7) with Eqs. (8) and (11), we will obtain the expression for the accelerometer's overall input noise acceleration spectral density a_n [16]:

$$\overline{a_n{}^2} = 4kT\left\{\frac{\eta C_{PE}}{\omega Q_{PE}{}^2} + \frac{0.01\omega_0}{mQ} + \frac{\Gamma}{g_{fs}V_{PE}{}^2} + \frac{R_b C_f{}^2}{[1+(\omega R_b C_f)^2]Q_{PE}{}^2}\right\} + \frac{\alpha q V_G{}^*}{2C_{in}fV_{PE}{}^2} + \frac{2qI_{GSS}}{(\omega Q_{PE})^2}. \quad (12)$$

In Eq. (12), the first two terms correspond to the PE transducer's electrical-thermal noise and mechanical-thermal noise, respectively. The third and fourth terms represent the amplifier's FET thermal noise of and the noise generated by the resistor R_b, respectively. The fifth and sixth terms define the amplifier's FET 1/*f* noise and the shot noise in the input gate circuit, respectively. Expression (12) identifies the parameters of the accelerometer providing ultra-low-noise operation.

The spectral noise of the Meggitt (OC) accelerometer model 86 was estimated according to the expression (12). At this estimate, the noise of the PE transducer a_{nPE} was calculated using Eq. (8) and the charge amplifier noise a_{namp} was measured directly with the help of the Hewlett Packard 3562A dynamic analyzer [15, 16]. At this measurement, the equivalent capacitance equaled to the PE transducer's capacitance C_{PE} was connected in parallel with the amplifier's input instead of PE transducer.

It is known that the direct measurement of the designed accelerometers' noise is not possible in a typical laboratory condition because of the influence of environmental vibration noise and the interferences always presented under such conditions. The model 86 estimated values of noise were verified in the NIST by the direct measurement of its noise using the NIST stabilization platform. Isolation of the sensor from the environmental vibration noise sources was provided [17]. **Figure 10** shows noise curves of the Meggitt (OC) model 86: estimated noise (curve 1) and experimental noise (curve 2) measured in NIST at frequencies from 0.1 to 100 Hz [17]. We can see that noise values have a good correlation with each other.

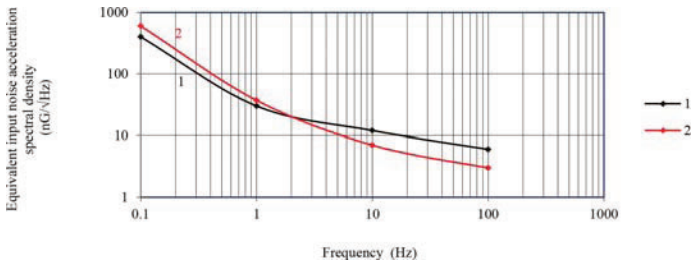

Figure 10. Noise of the Meggitt (OC) model 86: modeled (curve 1) and experimental (curve 2) measured in NIST [17].

5. Comparison of the designed accelerometers with the state-of-the-art low-noise seismic accelerometers

Table 2 shows a comparison between performance characteristics of the designed IEPE accelerometers Meggitt (OC) models 86, 87-10, and the state-of-the-art low-noise IEPE and MEMS accelerometers. These sensors are the IEPE sensors: Meggitt (MD) model 731A, PCB model 393B31, and Dytran model 3191A1 [11, 12, 14]. The MEMS sensor is the Colibrys model SF3000 [19]. Parameters of these sensors were obtained from their respective data sheets [11, 12, 14, 19].

			IEPE seismic accelerometers				MEMS
Parameters	**Units**	**Meggitt (OC)86**	**Meggitt (OC) 87-10**	**Meggitt (MD) 731A**	**PCB v393B31**	**Dytran 3191A1**	**Colibrys SF3000L**
Sensitivity	V/G	10	10	10	10	10	1.2
Range	±G	0.5	0.5	0.5	0.5	0.5	3
Frequency range (–3 dB)	Hz	0.003–200	0.02–500	0.05–450	0.04–500	0.045–1000	0–1000
Resonant frequency	Hz	370	1220	750	700	8000	
Temperature range	°C	−20– +100	−20– +100	−10– +65	−18– +66	−51–121	−40– +85
Output bias	V_{dc}	9–13	9–13	9	8–14	11–13	±0.24
R_{out}	Ω	≤10	≤10	100	500	100	
Full scale output	±V	5	5	5	5	5	3.6
Spectral noise	$nG/\sqrt{Hz}$						
0.1 Hz		600	800				
1 Hz		37	90	60	60	310	
10 Hz		7	25	10	10	150	300–500
100 Hz		3	10	4	4	61	300–500
Voltage supply	V_{dc}	24–30	24–30	18–30	24–28	18–30	±6– ±15
Current supply	mA	2–10	2–10	2–10	2–10	2–20	30
Shock limit	G pk	250	400	15	40	100	1000
Dimensions:	mm						
Diameter	mm	64.8	28.6	62	57	50	
Height	mm	55.5	37.3	53	53	92	
Weight	g	771	170	775	635	760	455

Table 2. Comparison between performance characteristics of the designed accelerometers, Meggitt (OC) models 86, 87-10, and the state-of-the-art IEPE and MEMS seismic low-noise accelerometers.

Figure 11 shows curves of the noise floor in terms of the equivalent input acceleration spectral density (in $nG/\sqrt{Hz}$) of the deigned models 86 and 87-10 (curves 1 and 2, respectively) and the

state-of-the-art models mentioned above (curves 3–6). Curve 3 shows the noise of the PCB model 393B31 and Meggitt (MD) model 731A (these models have about the same noise). Curves 4 and 5 represent noise of the Colibrys model SF3000L and Kistler model 8330A3, respectively. Curve 6 corresponds to the Dytran IEPE model 3191A1.

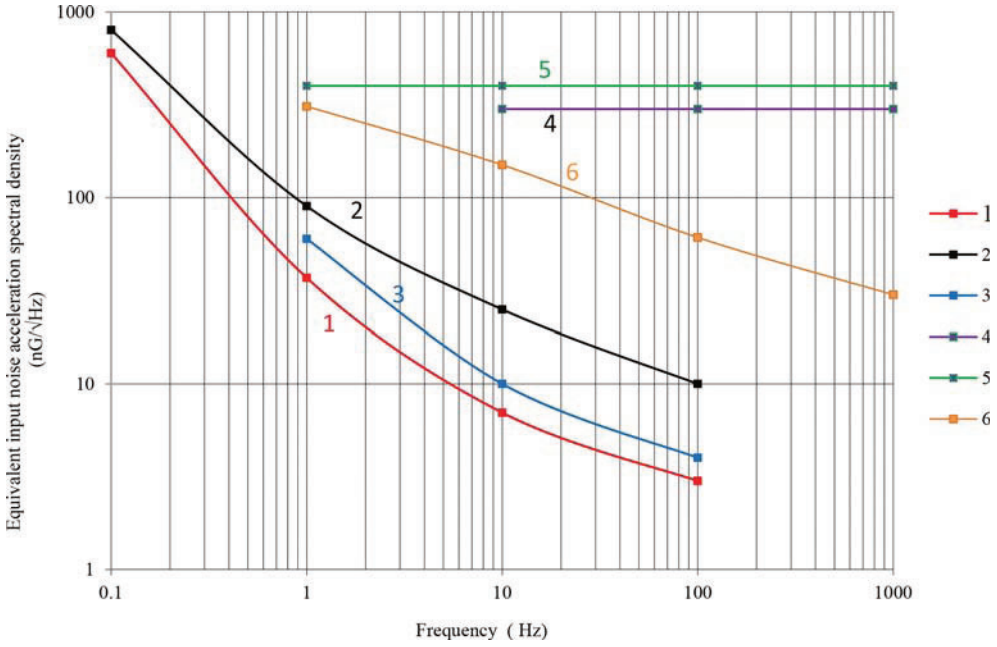

Figure 11. Comparison of the noise floor between the designed accelerometers, Meggitt (OC) models 86, 87-10, and the state-of-the-art low-noise seismic accelerometers. (1) model 86, (2) model 87-10, (3) Meggitt (MD) model 731A and PCB model 393B31, (4) Colibrys model SF3000L, (5) Kistler model 8330A3, and (6) Dytran model 3191A1. Values of noise in (3)–(6) are obtained from their respective data sheets [11, 12, 14, 18].

The designed sensors, models 86 and 87-10, have probably the lowest noise floor for their size and weight to date, in comparison to the existing state-of-the-art seismic accelerometers. Specifically, the model 86, having sensitivity size and weight comparable with the IEPE sensors PCB model 393B31 and Meggitt (MD) model 731A, has noise in terms of $nG/\sqrt{Hz}$ less than these sensors by factor of about 1.6 (about 2.6 in terms of power spectral density, nG^2/Hz) at frequency 1 Hz and by factor of about 1.4 in $nG/\sqrt{Hz}$ (about 2 in terms of nG^2/Hz) at frequencies 10–100 Hz. We can expect that the noise of the model 86 is less than the noise of these sensors by a factor > 2 in $nG/\sqrt{Hz}$ (>4 in nG^2/Hz) at frequencies $f < 1$ Hz.

The noise of the model 87-10 cannot be compared to any other IEPE seismic accelerometers' noise because they are not comparable in size and weight.

In addition to ultra-low-noise, the models 86 and 87-10 have lower operating frequencies (0.003 Hz for the 86 and 0.02 Hz for the 87-10 at the level of –3 dB vs. 0.05 Hz for the 731A and 0.04 Hz for the 393B31), higher operating temperature (T_{max} = 100°C vs. 65°C), less output

http://dx.doi.org/10.5772/65925

impedance ($R_{out} \leq 10\Omega$ vs. 100 and 500Ω), and higher shock limit (250 and 400 G pk vs. 15 and 40 G pk), in comparison to the existing state-of-the-art IEPE accelerometers.

6. Conclusion

Earthquakes can be so small or distant that only ultra-low-noise sensors are capable of measuring and monitoring small acceleration signals generated by such earthquake. In addition, such sensors can be used for the warning prediction system by detecting and monitoring of "preseismic" small changes on the ground that indicate that a significant quake is imminent. The Meggitt (OC) ultra-low-noise IEPE seismic accelerometers models 86 and 87-10 featuring probably the lowest noise (for its size and weight) and lowest operating frequencies (near dc) ever reported to date among these types of sensors are the best candidates for such purposes. The design and characteristics of these sensors are presented. The model 86 has a weight of about 770 g and a frequency range from 0.003 to 200 Hz at the ±3 dB level. Its noise in terms of the equivalent input noise acceleration spectral density is about 37, 7, and 3 nG/ $\sqrt{\text{Hz}}$ at frequencies 1, 10, and 100 Hz, respectively. The model 87-10 is a compact sensor with a weight of about 170 g and a frequency range from 0.02 to 500 Hz at the ±3 dB level. It has noise of about 90, 25, and 10 nG/$\sqrt{\text{Hz}}$ at frequencies 1, 10, and 100 Hz, respectively. The noise of the model 86 was directly measured at the National Institute of Standards and Technology (NIST). The noise measurement results have a good correlation with the sensor's noise theoretical estimation. In addition to the ultra-low-noise and near-dc frequency response, the designed accelerometers feature about six times higher shock limit, about 1.5 times higher temperature range, and one order of magnitude less output impedance, in comparison to the similar IEPE seismic accelerometers.

These sensors can be used in the seismic network capable of detecting microseismic fluctuations. The warning system using these sensors would be fundamentally different from current warning systems using the network of hundreds of seismometers across seismically active regions and recording only seismic events.

Author details

Felix A. Levinzon

Address all correspondence to: felix.levinzon1@meggitt.com

Meggitt (Orange County) Corporation, Irvine, CA, USA

References

[1] F. Niu, et al. "Preseismic velocity changes observed from active source monitoring at the Parkfield SAFOD drill site," *Nature Letters*. vol. 454, pp. 204–209, 2008.

[2] L. Chang-Peng and L. Li-Li, "Real time detection for anomaly data in microseismic monitoring systems," in *Proc. Int. Conf. Comput. Intell. Nat. Comput*., Wuhan, China, pp. 307–3010, 2009.

[3] A. Holland, "Earthquake data recording by MEMS accelerometer: Field testing in Idaho," *Seismological Research Letters*, 2003, DOI: 10.1785/gssrl.74.1.20.

[4] X. Cheng, et al. "Similar microearthquakes observed in western Nagano, Japan, and implications for rupture mechanics," *Journal of Geophysical Research*, 112, B04306, 2007, DOI:10.1029/2006JB004416.

[5] T. Taka'aki, et al. "Remote triggering of fault-strength changes on the San Andreas fault at Parkfield," *Nature Letters*, 461/1, 636–639, 2009, DOI: 10.1038/nature08395.

[6] A. Zollo, et al. "A threshold-based earthquake early warning using dense accelerometer networks," *Geophysical Journal International*, 183(2), 963–974, 2010.

[7] E.S. Cochran, et al. "The Quake-Catcher Network: Citizen expanding seismic horizons," *Seismological Research Letters,* 2009, DOI: 10.1785/gssrl.80.1.26.

[8] N. Maercklin, et al. "The effectiveness of a distant accelerometer array to compute seismic source parameters: the April 2009 L'Aquila warthquake case history," *Bulletin of the Seismological Society of America*, 101(1), 354–365, 2011.

[9] J. Geng, et al. "A new seismogeodetic approach applied to GPS and accelerometer observations of the 2012 Brawley seismic swarm: Implications for earthquake early warning, "*Geochemistry, Geophysics, Geosystems*, 14(7), 2124–2142, 2013.

[10] *Model 86 Seismic accelerometer, Specification Sheet*, Meggitt (OC), Endevco, CA, https://www.endevco.com/86/ [Internet].

[11] *Seismic accelerometer model 731A, Data sheet, rev. C6*, Meggitt (MD), Wilcoxon Research, Germantown, MD, 2010, http://www.wilcoxon.com/prodpdf/731A%20spec%20(98078C6).pdf [Internet].

[12] *Seismic accelerometer model 393B31, Specifications*, PCB Piezotronics, Depew, NY, http://www.pcb.com/products.aspx?m=393B31 [Internet].

[13] *Model 87 Seismic accelerometer, Specification Sheet,* Meggitt (OC) Endevco, CA, https://www.endevco.com/87-10/ [Internet]

[14] *Model 3191A1, Performance Specifications*, Dytran Instruments, Chatsworth, CA, http://www.dytran.com/Assets/PDF/3191A1_ds.pdf [Internet].

[15] F.A. Levinzon, "Ultra-low-noise seismic piezoelectric accelerometer with integral FET amplifier," *IEEE Sensor Journal*, 12(6), 2012.

[16] F.A. Levinzon, "Piezoelectric Accelerometers with Integral Electronics," Chapter 8, 135–149, Springer, 2015, DOI: 10.1007/978-3-319-08078-9.

[17] F.A. Levinzon and R.D. Drulinger, "The industry's lowest noise 10 V/G seismic accelerometer," presented at the IMAC 26th International Conference, Orlando, FL, Feb. 2008.

http://dx.doi.org/10.5772/65925

[18] *Servo-Beam Accelerometer Type 8330A3, Data Sheet*, Kistler, Amherst, NY, 2006.

[19] *Seismic Accelerometer SF3000L, Data Sheet*, Colibrys Inc., Neuchatel, Switzerland, http://www.colibrys.com [Internet]

[20] L.M.W. Brownjohn, "Practical considerations for low noise measurements," Dept. Civil Structural Engineering, University of Sheffield, UK. http://studylib.net/doc/8766249/practical-considerations-for-low-noise-measurement--j.m.w. [Internet].

[21] A. Bertolini, et al. "Monolithic folded pendulum accelerometers for seismic monitoring and active isolation systems," *IEEE Transactions on Geoscience and Remote Sensing*, 44(2), 273–276, 2006. http://authors.library.caltech.edu/5606/ [Internet].

[22] S. Saponara, et al. "Modeling, sensitivity analysis, and prototyping of low-g acceleration acquisition systems for spacecraft testing and environ mental-noise measurements," *IEEE Transactions on Instrumentation and Measurement*, 60(2), 385–397, 2011.

[23] R.C. Snel, J.G. Mangum, J.W.M. Baars, "Study of the dynamics of large reflector antennas with accelerometers," *IEEE Antennas and Propagation Magazine*, 49(4), 84–101, 2007.

[24] C.P. Germano, *Flexure Mode Piezoelectric Transducers*. Morgan ElectroCeramic, Stourport, UK, http://www.morgan-electroceramic.com [Internet].

[25] F.A. Levinzon, "Noise of piezoelectric accelerometer with integral FET amplifier, *IEEE Sensors Journal*, 5(6), 1235–1242, 2005.

[26] F.A. Levinzon, "Fundamental noise limit of piezoelectric accelerometer," *IEEE Sensor Journal*, 4(1), 108–111, 2004.

[27] A.J. Scholten, et al. "Noise modeling for RF CMOS circuit simulation," *IEEE Transactions on Electron Devices*, 50, 618–632, 2003.